Supporting Information

Wood-templated Unidirectional Piezoceramic Composite for Transmuscular Ultrasonic Wireless Power Transfer

Ying Hong,[†a] Lihan Jin,[†a] Biao Wang,[†a] Junchen Liao,[b] Bing He,[c] Tian Yang,[c] Zhihe Long,[a] Pengyu Li,[a] Zhuomin Zhang,[a] Shiyuan Liu,[a] Youngjin Lee,[c] Bee Luan Khoo,[b, d] Zhengbao Yang *[a]

This file includes:

Supplementary Methods

Supplementary Figures

Supplementary Tables

Captions for Supplementary Videos S1 to S4

Other Supplementary Materials for this manuscript includes the following:

Supplementary Videos S1 to S4

Supplementary Methods

1. Finite element simulation

To gain an insight into the working mechanism of the proposed W-PUEH device, we perform a finite element analysis (FEA) using a commercially available software COMSOL. The physical parameters of water, PDMS and PZT-5H are selected from the material library in COMSOL. Cuboid water with $70 \times 70 \times 18.5$ cm^3 volume is modeled and an ultrasound probe with different diameters is centered at the surface of the water. The $3.0 \times 3.0 \times 0.5$ cm^3 porous device is enveloped by a $3.1 \times 3.1 \times 0.6$ cm^3 PDMS. The device is laid under the ultrasound probe. In the FEA simulation, the electrode layers of the device are not taken into account. The frequency of the ultrasound probe is set to 40 kHz. To investigate the acoustic, mechanical and piezoelectric interactions in the system, we use pressure acoustics, solid mechanics and electrostatics physics and set the corresponding acoustic-structure boundary and piezoelectric effect.

To compare the performance of the W-PUEH device with 1-3 PZT composites and bulk-based PZT composites, we also build the models for these two cases in Fig. S1. In three models, the thickness and volume of PZT, the size of PDMS matrix and the physical conditions keep the same as those of the W-PUEH device. The 1-3 composite contains 9 units with the $0.75 \times 0.75 \times 0.5$ cm^3 volume. The gap between the adjacent units is set to 1 cm. Fig. S1 shows the acoustic field and corresponding potential when the potential reaches its maximum. The finite element simulation shows that the 1-3 PZT composite and wood-templated PZT composite exhibit higher voltage output than the bulk-based PZT composite. Besides, the PZT core element of 1-3 PZT composite and wood-templated PZT composite is geometrically complementary, indicating that the designed wood-templated aligned framework structure is an essential supplementary to 1-3 composites in ultrasonic energy transfer. Compared to 1-3 composites, the W-PUEH has the advantage of easy fabrication, low cost and massive production.

To further analyze the influence of the ultrasound probe size on the acoustic field and electrical output, the ultrasonic pressure propagation and corresponding piezoelectric potential distribution inside the W-PUEH with different probe size is also simulated. Fig. S2 shows the acoustic field and corresponding potential when the ultrasound wave propagates to the W-PUEH surface and when the potential reaches its maximum, respectively. In the case where the probe size is smaller than the sample size, the acoustic pressure applied to the sample surface in different regions are obviously non-uniform and the strain near the sample edge is larger than that in the center region of the sample, leading to the decrease of the voltage output. On the other hand, in the case where the probe size is larger than the sample size, serious interference occurs when the reflected acoustic wave with various phases outside the sample region interferes with the incident wave, degrading the voltage output. As a result, when the dimension of the ultrasound probe (15 mm radius) is close to the W-PUEH device (3.0×3.0 cm^2), the W-PUEH device produces the largest voltage output, as shown in Fig. 1d.

The electrical impedance spectrums for the W-PUEH, 1-3 composite, and bulk PZT are also simulated. The water and PDMS matrix are removed in the simulation. A constant damping ratio is introduced and set to 0.15 for the three cases. From Fig. S7, we can observe that both planar and thickness resonance modes exist in the W-PUEH and bulk PZT, while only thickness resonance mode is seen in 1-3 composite. Besides, the resonant frequencies in the planar resonance modes for the W-PUEH are significantly depressed compared to bulk PZT. The resonant frequency in the thickness mode is around 310 kHz.

2. The manufacturing procedure of the W-PUEH device

Preparation of the PZT [Pb(Zr$_{0.52}$Ti$_{0.48}$)O$_3$] sol solution

The flexible piezoelectric wood is manufactured by a modified template-assisted sol-gel method (Fig. 2a). To fabricate PZT [$Pb(Zr_{0.52}Ti_{0.48})O_3$] sol solution, lead (II) acetate trihydrate (99%, Alfa Aesar), zirconium (IV) propoxide (70 wt% in 1-propanol, TCI), titanium (IV) butoxide (99%, TCI) and acetic acid (99%, Dieckmann) are prepared as the starting materials. The lead (II) acetate trihydrate with a 20% excess is firstly distributed in acetic acid under magnetic stirring at 70 °C until fully dissolved. After cooling down to room temperature, the zirconium (IV) propoxide is dropped slowly into the prepared solution under vigorous stirring, followed by titanium (IV) butoxide. The concentration of the final PZT sol is 2 M, with a molar ratio of Pb : Zr : Ti =1.2 : 0.52 : 0.48. A 20% excess of Pb is used for the compensation of lead volatilization in high temperatures. Fully stirring for 0.5 hour, ethylene glycol (99.5%, Dieckmann) is then added to the prepared solution to stabilize the PZT sol solution.

Preparation of the PZT sol-powder suspension

The introduction of PZT powders in the preparation of PZT sol-powder suspension aims to increase the effective mass and wall thickness of the PZT ceramic framework in the composite, further enhancing the piezoelectric responses. And the added PZT powders will not destruct the perovskite structure of the PZT ceramic framework, which is confirmed through the X-ray diffraction (XRD) patterns (Fig. S6a) and the Raman spectrum (Fig. S6b).

To prepare the PZT sol-powder suspension, PZT powders need to be modified first. The purchased PZT powders (Yisheng Electronics Co., Ltd, Xi'an) and polyethyleneimine (PEI, Aldrich) are distributed in distilled water separately. Then the prepared PEI solution is added slowly to the dispersed PZT-water suspension with vigorous stirring. After fully stirring, the surface-modified PZT powders are successfully separated by centrifugation, and the extra PEI solution is washed away by distilled water. After the hydrophilic treatment mentioned above, the surface-modified PZT powders are dispersed in the prepared PZT sol solution (1:1 mass ratio). After stirring for 2 hours, the well-dispersed PZT suspension is obtained.

Preparation of the chemical-treated wood template

The prepared balsa wood is immersed in the boiling hydrogen peroxide (H_2O_2, 30%, Anaqua) for about 3 h until the color of the wood turns from brown to pure white. Then the chemical-treated wood template is immersed in the boiling water for 0.5 hours to remove residual H_2O_2. After washing in boiling water for 3 times, the prepared wood template is dried in a freeze dryer for 1 day. Finally, the chemical-treated wood template is obtained.

Preparation of the W-PUEH device

The prepared chemical-treated wood template is immersed in PZT suspension until the whole wood template is infiltrated with the PZT suspension within a few seconds. After squeezing to remove extra PZT suspension, the sample is dried in an oven at 70°C for 1 hour. With the sol immersed in the wood template converting to gel, the precursor is sintered in 1000°C for 2 hours at Pb atmosphere to remove the wood template. Finally, the aligned lamellar piezoelectric framework is obtained. During sintering, the porous structure of the PZT framework greatly decreases the thermal stress during sintering and allows the framework deformation to some extent, which helps the prevention of fracture. As a result, it is more flexible for the parameter requirement in the sintering process and we set the heating rate as 15 °C/min.

To prepare the W-PUEH device, the uncured polydimethylsiloxane (PDMS, Sylgard 184, Dow Corning Co., Ltd) with 10wt% curing agent is fully mixed and then vacuumed to remove the bubble. Then the prepared piezoceramic framework is immersed in uncured PDMS until the piezoceramic framework is fully infiltrated with uncured PDMS. After curing at 70°C for 2 h, the wood-templated piezoelectric composite is finally obtained. With silver film sputtered as the electrode and PDMS film spin-coated as the protective layer, the prepared W-PUEH is polarized at 85°C for 1 hour under the electric field of 15 kV/mm and then naturally cooled down to room temperature.

3. Materials characterization and piezoelectric performance characterization

The scanning electron microscopic morphologies from natural wood to piezocomposite are examined by a scanning electron microscope (JEOL, JSM-5600). The energy dispersive spectroscopic (EDS) mapping of the PZT piezoceramic framework is characterized by an energy dispersive spectrometer (Oxford Instruments, INCA Energy 200). The crystal structures of the PZT ceramic are characterized by X-ray diffraction (XRD, Rigaku SmartLab). The Raman spectrum of the PZT ceramic is characterized by a Raman spectrometer (Perkinelmer Raman station 400F).

PFM is conducted on the W-PUEH composite with a BRUKER Dimension Icon system. The probe used is a Bruker's MESP-RC-V2 with Co/Cr conductive coating, nominal stiffness of 5 N/m, and nominal resonance frequency of 150 kHz. For characterization of PFM amplitude and phase, a small area (5×5 μm^2) is scanned in Low Speed Mode with low frequency (15 kHz) to avoid contact resonance (typically around 300 kHz).

The ferroelectric hysteresis is characterized by a ferroelectric analyzer (Mutiferroic, RADIANT). The Young's modulus of the piezocomposite is measured by a mechanical testing platform. The piezoelectric coefficient d_{33} of the piezocomposite is measured by a d_{33} meter (YE2730A, Sinocera).

The pressure sensitivity measurement of the W-PUEH device is conducted by a vibration generator, with a controllable oscillation frequency and compressing force. The compressing force, detected and quantified by a mechanical force sensor, is adjusted by the distance between the taping pillar and sample surface. The piezoelectric output voltage and current are measured by a digital oscilloscope (Rohde & Schwarz RTE1024) and a low-noise current preamplifier (Stanford Research SR570), respectively.

The ultrasonic-induced outputs of the W-PUEH device are characterized by an assembled testing platform. The W-PUEH device (ultrasonic receiver) is placed in a water tank, close to a fixed PZT transducer (ultrasonic transmitter). The distance between the transmitter and the receiver is controlled by a lifting platform below the water tank. In frequency-dependent characterization, the transmitter is actuated by a function generator (DG1062Z, Rigol) and an amplifier (4090, Dongjia). In the electrical characterization with constant input frequency, the transmitter is driven by an ultrasonic generator (K3, KMD) with high input power. The input power intensity is measured by a hydrophone (J100E, CYS).

4. Wireless signal transmission

To show the power-generation ability of the energy harvester for the sensors *ex vivo*. We power a wireless temperature monitoring system in which the transmitter sends a real-time radio frequency signal obtained by a temperature sensor integrated with the transmitter. The detailed process is described as follows. A full-bridge rectifier is firstly connected to the W-PUEH device for rectifying the alternating current (AC) to the direct current (DC). Then, a 330 µF capacitor stores the converted energy. To guarantee that the wireless MCU with the working voltage of 1.7 V is activated with enough energy gathered in the capacitor to complete a successful signal transmission, we insert an under-voltage lockout (UVLO) module between the full-bridge rectifier and the wireless transmitter. And the rising switching-on and falling switching-off voltages are set to 2.0 V and 1.7 V respectively. After the completion of the signal transmission, the corresponding wireless receiver reads out the data and sends it to the computer for display through the USB serial port. In the experiment, we use the integrated temperature sensor to detect the temperature variation of the palm surface every 6 seconds, and the captured temperatures are ~ 34 ℃, ~ 36.5 ℃, and ~ 38 ℃, respectively.

5. Animal preparation

All experimental and surgical procedures are conducted according to the Institutional Animal Care and Use Committee (IACUA) guidelines, reviewed and approved by the Animal Research Ethics Sub-Committee in City University of Hong Kong and Department of Health, Government of the Hong Kong Special Administrative Region. A male ICR mouse (9 weeks, weighing approximately 40g) is purchased from the Laboratory Animal Research Unit (LARU) of City university of Hong Kong. Before the experiment, the mouse is anesthetized with an intraperitoneal injection of Ketamine/Xylazine mixture (80 mg/kg body weight ketamine and 10 mg/kg body weight xylazine). Before implanting the W-PUEH, the hair in lower half of the abdomen is removed carefully with a shaver. A 15 mm midline skin incision is made in the lower abdomen of the mouse. The skin is detached from the muscle to create a pocket for the W-PUEH. The device is inserted into the pocket, leaving the wire outside the body for transmitting the electrical signals. The skin incision is closed with suture. After the experiment, mouse is sacrificed in a CO_2 chamber in accordance with laboratory protocols after the experiment.

6. Cell viability assay

1) Cell culture

The myofibroblast cell line WPMY-1 are purchased from American Type Culture Collection (ATCC) and cultured in Dulbecco's modified Eagle's medium (DMEM, Gibco, #11875085, USA) supplemented with 5% fetal bovine serum (FBS, Gibco, #10270106, USA) and 1% penicillin-streptomycin (Gibco, #15140122, USA). Cells are cultured under 5% CO_2 humidified atmosphere at 37 °C. Media are changed every 2 days and cells are passaged at 80% confluence.

2) Cell viability assay

PDMS, W-PUEH and PZT samples are placed in a 24-well plate and immersed in 75% overnight for sterilization. The samples are washed by PBS for three times to remove the residual ethanol. Myofibroblasts are digested and resuspended in fresh media. The cells are seeded into the 24 well plate at a density of $1.5 \times 10^4 \text{ml}^{-1}$ with 1 ml culture media. After 1, 3 and 5 days of incubation, the cells are stained with 5 μM Calcein AM (Invitrogen, #C3100MP, USA) under 37 °C for 20 min and 5 μM Propidium Iodide (PI) (Sigma-Aldrich, #81845, USA) at room temperature for 1 min to identify the live and dead cells. The stained samples are imaged with a fluorescence microscope (Nikon, Eclipse Ci-L, Japan).

3) Data and statistical analysis

All fluorescent images are processed by Image J software (National Institutes of Health, USA) and automated algorithms are generated to count both the cell numbers and fluorescent intensity from the derived images. The results are expressed as means ± standard deviation of three independent trials. One-way ANOVA and Student's t-test are conducted to evaluate associations between independent variables, and the statistical significance is defined as *$p<$ 0.01.

4) Results and discussion

At day 1, the three groups samples show the comparable cell viability (PDMS: 82.52 ± 6.63%, W-PUEH: 79.78 ± 5.34%, PZT: 81.43 ± 4.07%). However, the cell viability of the PZT samples keep decreasing in the following days (Day 3: 55.27 ± 7.16%, Day 5: 43.18 ± 7.15%), demonstrating the PZT samples produce a high cytotoxicity. It is observed that on the surface of the W-PUEH, the myofibroblasts exhibit a high proliferation rate (Fig. S21b) and the viability of the cells cultured on W-PUEH are still comparable to the PDMS control group (Fig. 6f) in day 3 (PDMS: 94.00 ± 1.74%, W-PUEH: 89.35 ± 5.78%) and day 5 (PDMS: 95.08 ± 0.35%, W-PUEH: 92.39 ± 1.47%), indicating the W-PUEH does not exhibit cytotoxicity and has a good biocompatibility.

Supplementary Figures
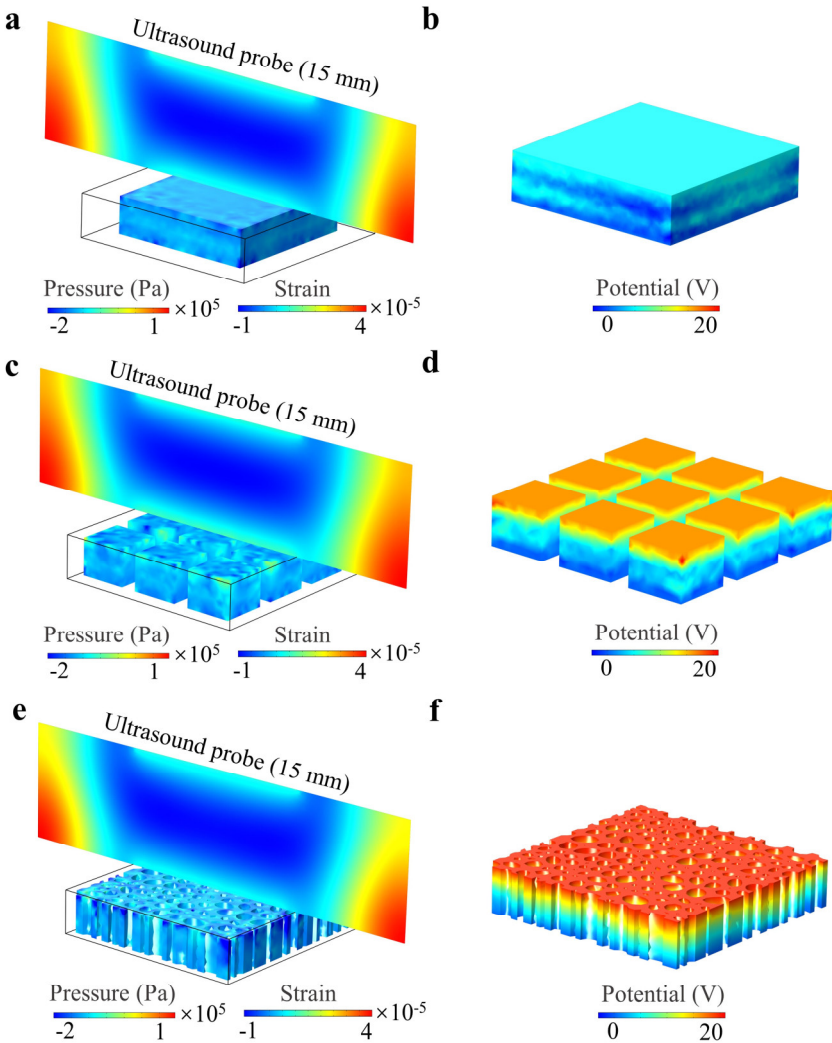
Fig. S1 Simulated acoustic field depending on the framework structure. (a and b) Finite element simulation of the acoustic field under water, strain distribution (a), potential distribution (b) in the bulk-based PZT composite when the potential reaches its maximum. (c and d) Finite element simulation of the acoustic field under water, strain distribution (c), potential distribution (d) in the 1-3 PZT composite when the potential reaches its maximum. (e and f) Finite element simulation of the acoustic field under water, strain distribution (e), potential distribution (f) in the wood-templated PZT composite when the potential reaches its maximum.
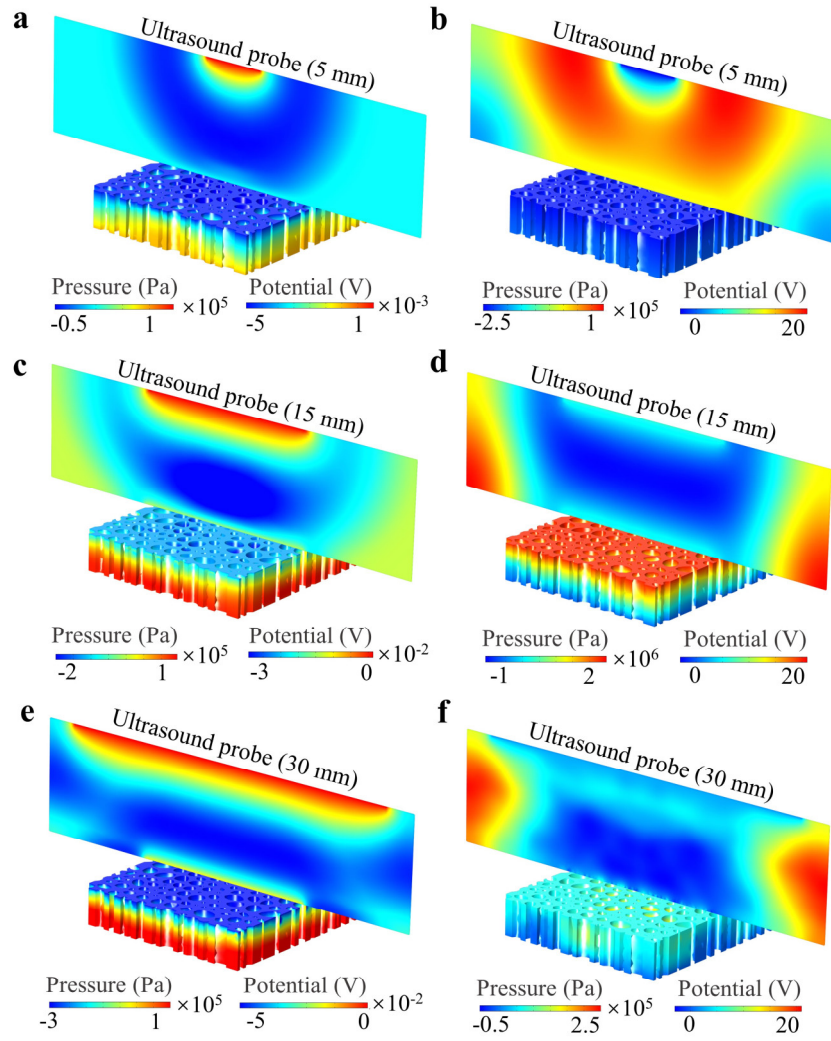
Fig. S2 Simulated acoustic field depending on the ultrasound probe size. (a and b) Finite element (FE) simulation of ultrasonic pressure propagation and corresponding piezoelectric potential distribution inside the W-PUEH when the ultrasound wave propagates to the W-PUEH surface (a) and the potential reaches its maximum (b), respectively. The radius of the ultrasound probe is 5 mm. (c and d) FE simulation when the ultrasound wave propagates to the W-PUEH surface (c) and the potential reaches its maximum (d), respectively. The radius of the ultrasound probe is 15 mm. (e and f) FE simulation when the ultrasound wave propagates to the W-PUEH surface (e) and the potential reaches its maximum (f), respectively. The radius of the ultrasound probe is 30 mm.
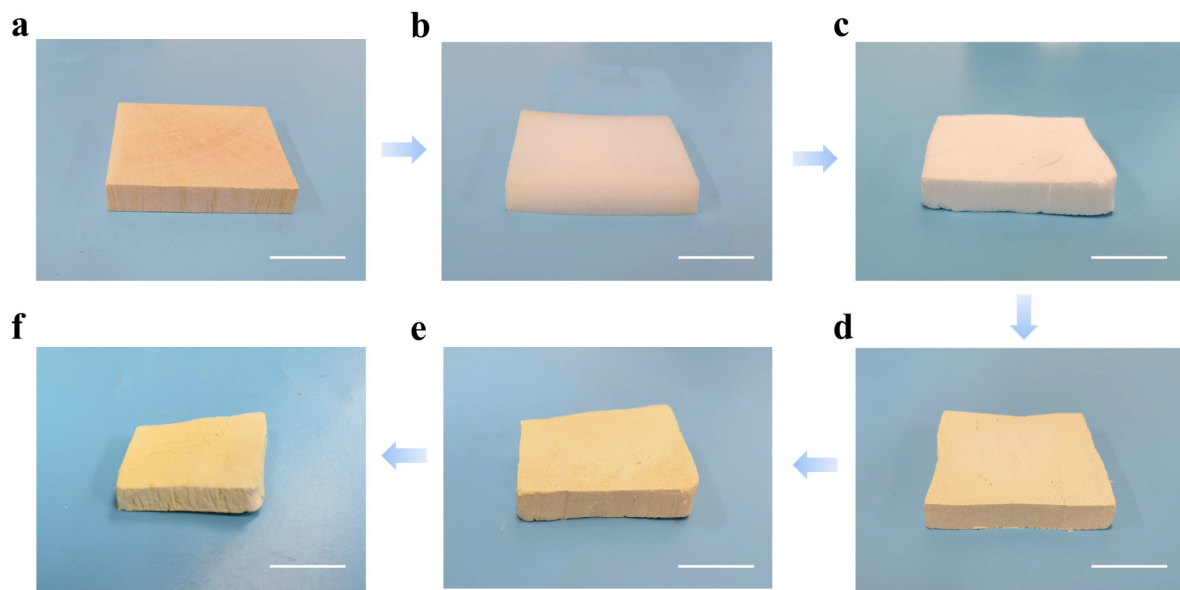
Figure S3. Optical images of the sample during the manufacturing from wood template to ceramic framework. (a) Balsa wood. (b) Chemical-treated wood. (c) Freeze-dried wood. (d) Precursor with PZT sol suspension immersed in the wood template. (e) Dried precursor. (f) Sintered ceramic framework. Scale bar, 2 cm.
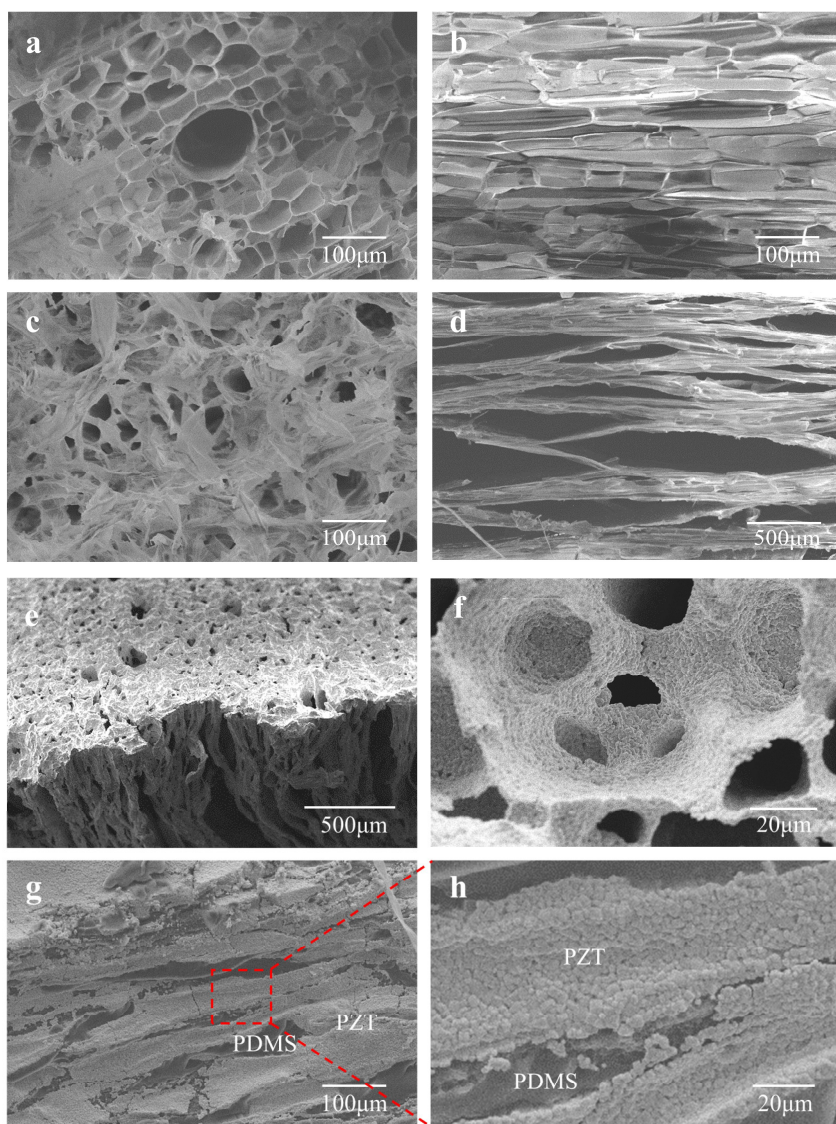
Fig. S4 Morphology characterization from wood template to piezocomposite. (a and b) Scanning electron microscopic (SEM) image of the natural wood in the transverse direction (a) and the longitudinal direction (b), showing the porous structure and lattice-like channels. (c and d) SEM image of the chemical-treated wood in the transverse direction (c) and the longitudinal direction (d), showing thinner cell walls and aligned lamellar microstructure. (e) Oblique SEM image of the piezoceramic framework. (f) Magnified SEM image of the piezoceramic framework, showing its porous microstructure. (g) SEM image of the piezocomposite in the longitudinal direction. (h) Magnified SEM image of the piezocomposite.
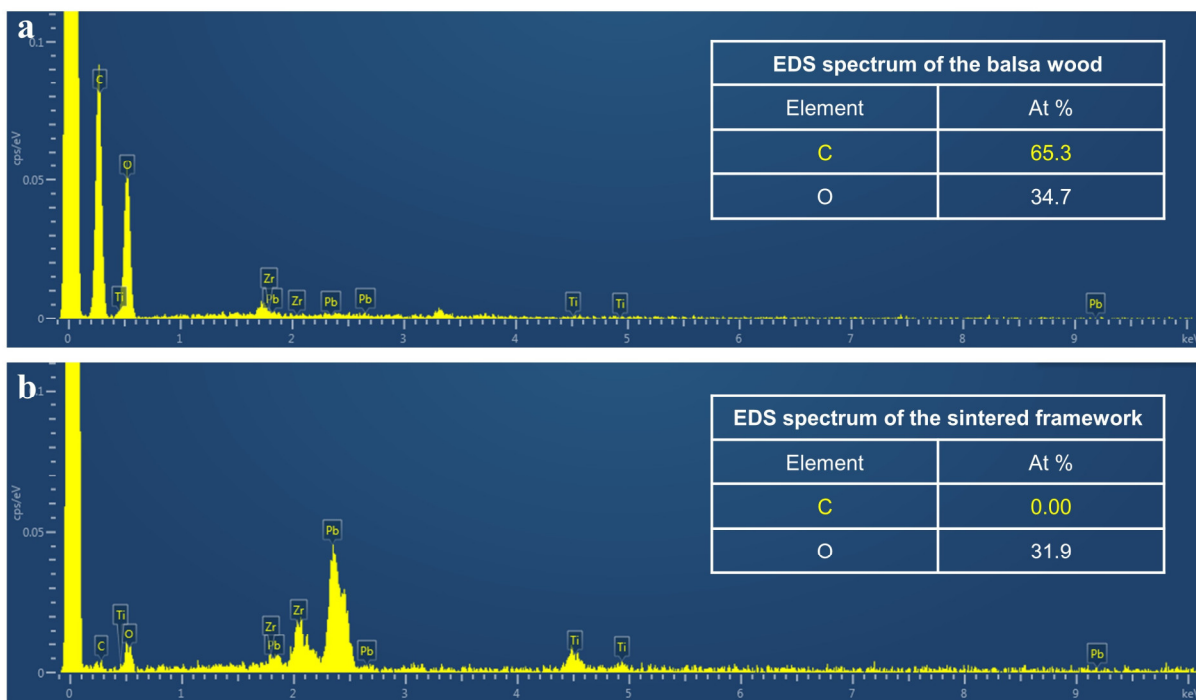
Fig. S5 EDS spectra of (a) the balsa wood and (b) the sintered ceramic framework. No characteristic peak of C element is detected in the sintered PZT skeleton, while which can be clearly observed in the wood, confirming the wood template is removed in the sintered PZT skeleton.
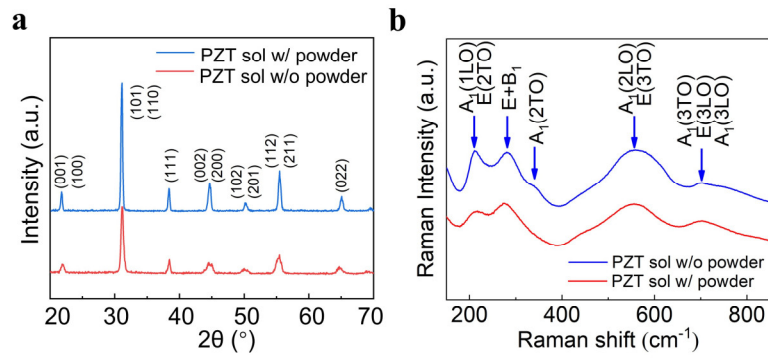
Fig. S6 Fundamental characterization of the W-PUEH. (a) X-ray diffraction (XRD) pattern of the piezoceramic framework based on the PZT sol solution with/without PZT powder. (b) Raman spectrum of the piezoceramic framework based on the PZT sol solution with/without PZT powder, showing a perfect perovskite structure.
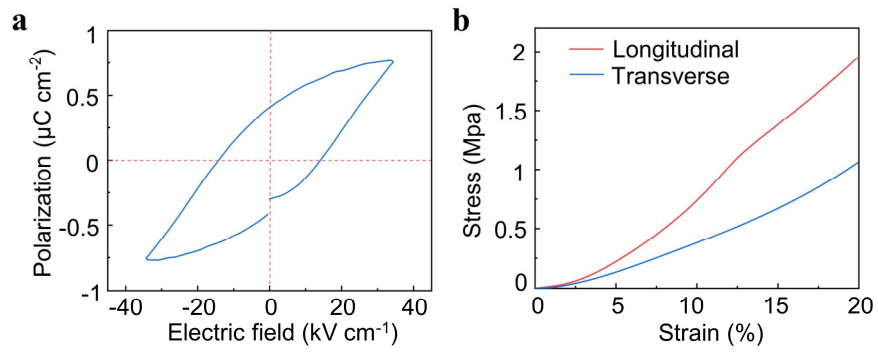
Fig. S7 (a) The polarization-electric field (P-E) loops of the W-PUEH along the longitudinal direction measured with a frequency of 10 Hz, showing a good ferroelectric hysteresis behaviour. (b) Stress-strain curves under compression for the wood-templated piezocomposite along the longitudinal direction and the transverse direction, respectively.
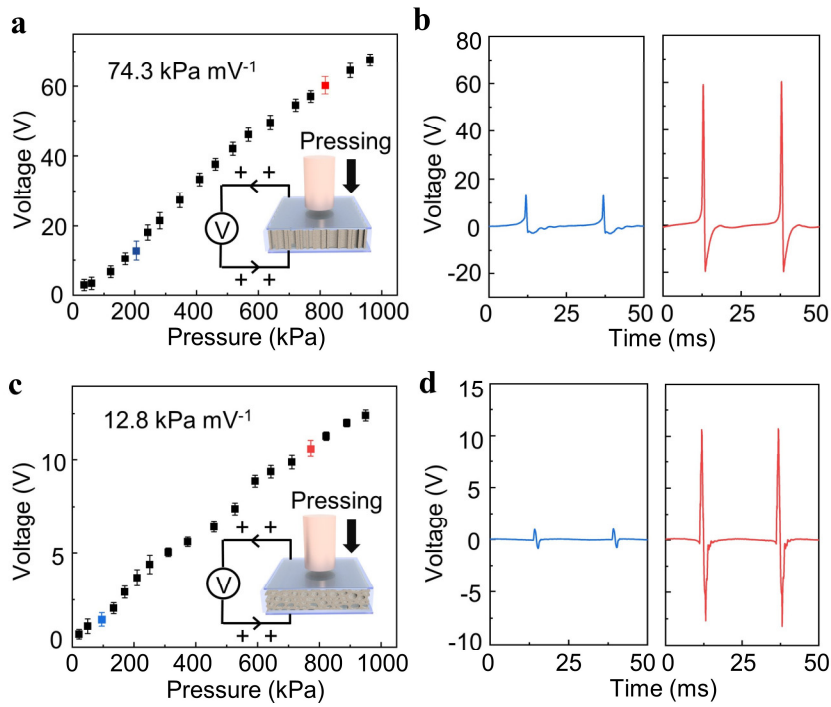
Fig. S8 Piezoelectric responses of the W-PUEH under compressive pressure. (a) The longitudinal output voltages of the W-PUEH under pressure from 0.02 MPa to 1 MPa. The load frequency is 40 Hz. Inset shows the current direction during the compression process. (b) Two typical voltage signals of the W-PUEH along the longitudinal direction under the pressure of 0.2 MPa and 0.8 MPa, respectively. (c) The transverse output voltages of the W-PUEH under pressure from 0.02 MPa to 1 MPa. The load frequency is 40 Hz. Inset shows the current direction during the compression process. (d) Two typical voltage signals of the W-PUEH along the transverse direction under the pressure of 0.1 MPa and 0.8 MPa, respectively.
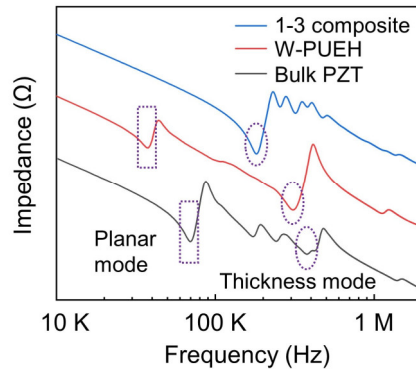
Fig. S9 FEM analysis of the vibration mode comparison between the 1-3 composite, W-PUEH and bulk PZT. The boxes indicate the first-order planar mode under resonant frequency and the circles indicate the first-order thickness mode under resonant frequency. Compared to bulk PZT, the low-frequency resonance at planar mode has been significantly depressed in W-PUEH, and the thickness resonance mode with resonance frequency around 310 KHz is seen.
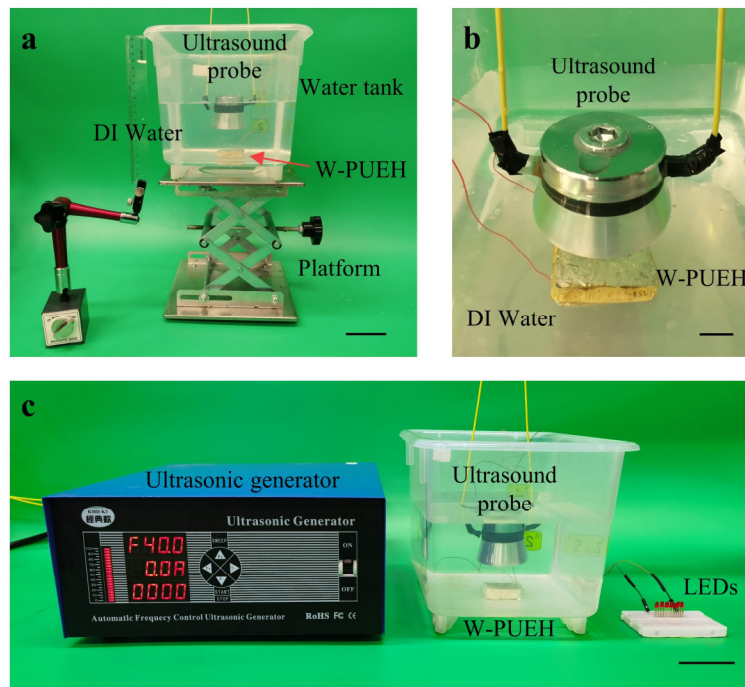
Fig. S10 Experimental setup. (a) Optical image of the experimental setup under water. Scale bar, 5 cm. (b) Magnified optical image of the transmitter and receiver. Scale bar, 1 cm. (c) Optical image of the experimental setup when lighting LEDs. Scale bar, 5 cm.
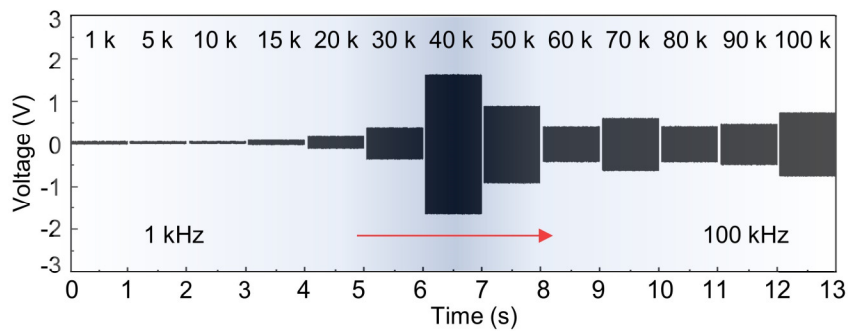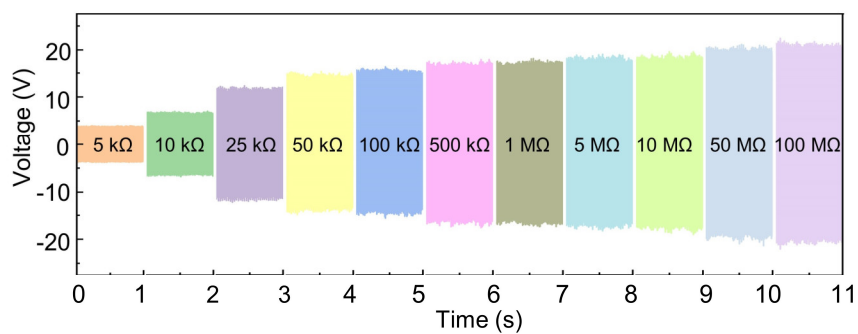
Fig. S11 Frequency-dependent characterization. Output voltage signals of the W-PUEH at the frequency ranging from 1 kHz to 100 kHz. The best performance appears at 40 kHz.
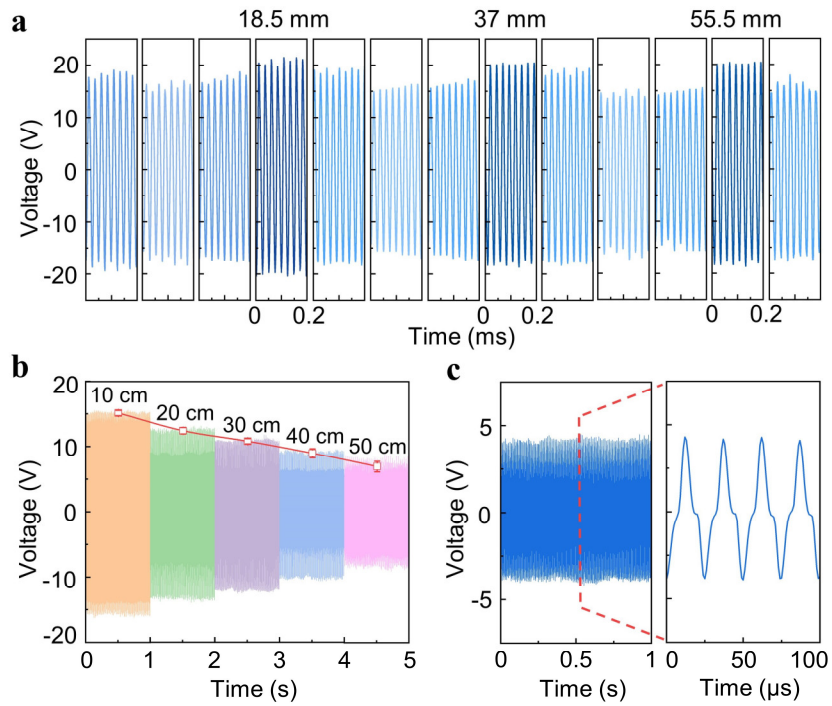
Fig. S12 Distance-dependent characterization. (a) Output voltage signals of the W-PUEH depending on the distance ranging from 5 mm to 59.5 mm. The setup of the ultrasonic transmitter is 40 kHz and 0.6 W cm^{-2}. (b) Open-circuit output voltage signals of the W-PUEH depending on the distance ranging from 10 cm to 50 cm. The setup of the ultrasonic transmitter is 40 kHz and 0.6 W cm^{-2}. (c) Output voltage signals generated by the W-PUEH at 25 kΩ when the distance is 50 cm. The setup of the ultrasonic transmitter is 40 kHz and 0.6 W cm^{-2}.
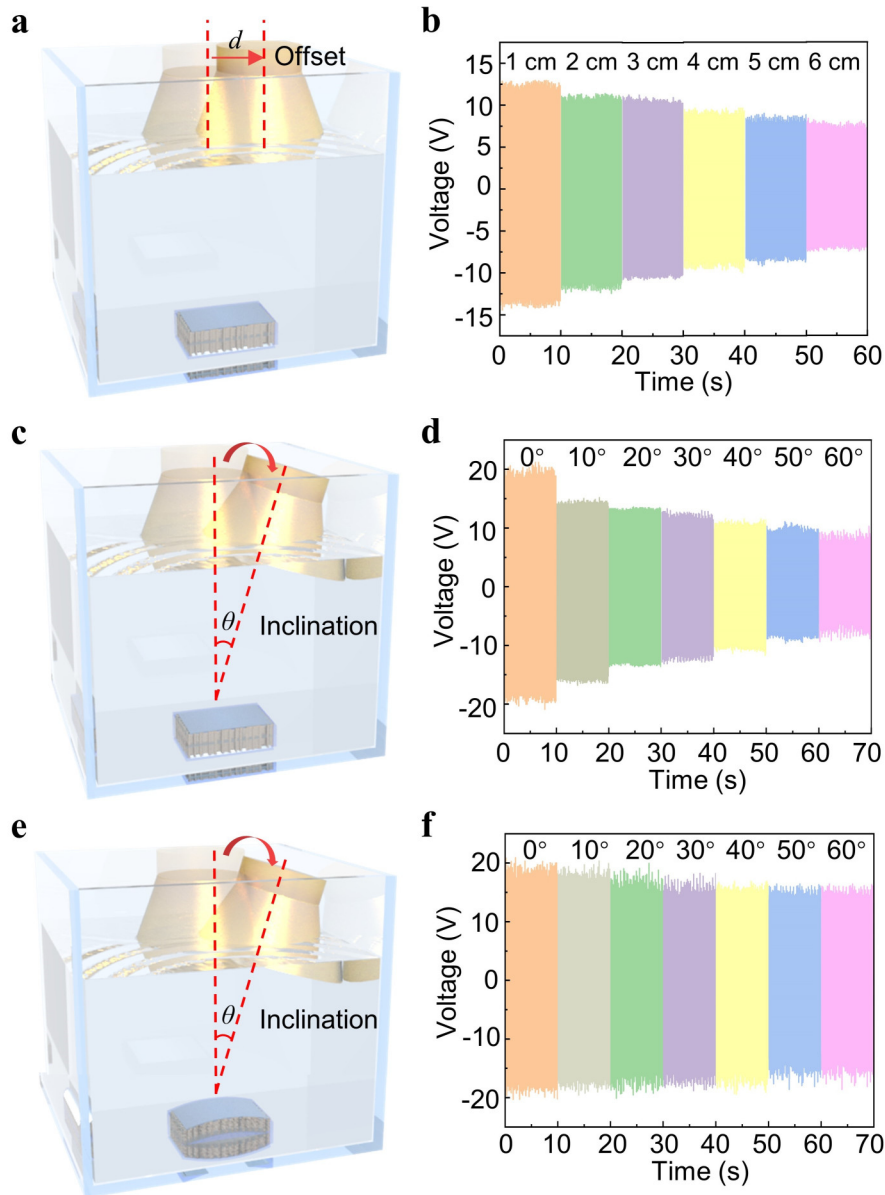
Fig. S13 Position-dependent characterization. (a and b) Output voltage signals of the flat W-PUEH depending on the offset distance of the transmitter with an input power of 0.6 W cm^{-2} and a frequency of 40 kHz. (c and d) Output voltage signals of the flat W-PUEH depending on the inclination angle of the transmitter with an input power of 0.6 W cm^{-2} and a frequency of 40 kHz. (e and f) Output voltage signals of the curved W-PUEH depending on the inclination angle of the transmitter with an input power of 0.6 W cm^{-2} and a frequency of 40 kHz.

Fig. S14 Impedance-dependent characterization. Output voltage signals of the W-PUEH depending on load resistance with a distance of 18.5 mm, an input power intensity of 0.6 W cm^{-2} and a frequency of 40 kHz.
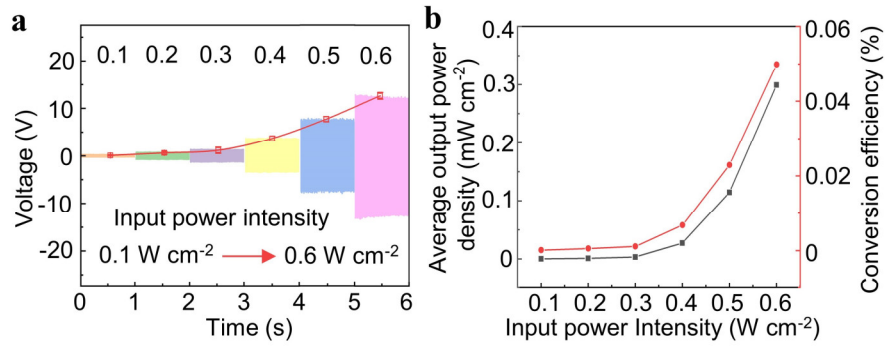
Fig. S15 Output power and conversion efficiency as a function of input power. (a) Output voltages of the W-PUEH depending on the input power (from 0.1 W cm^{-2} to 0.6 W cm^{-2}) of the transmitter with a distance of 18.5 mm and frequency of 40 kHz. The load resistance is 25 kΩ. (b) With input power increasing, the average output power density and conversion efficiency increase accordingly. The load resistance is 25 kΩ. The experimental setup is 18.5 mm and 40 kHz.
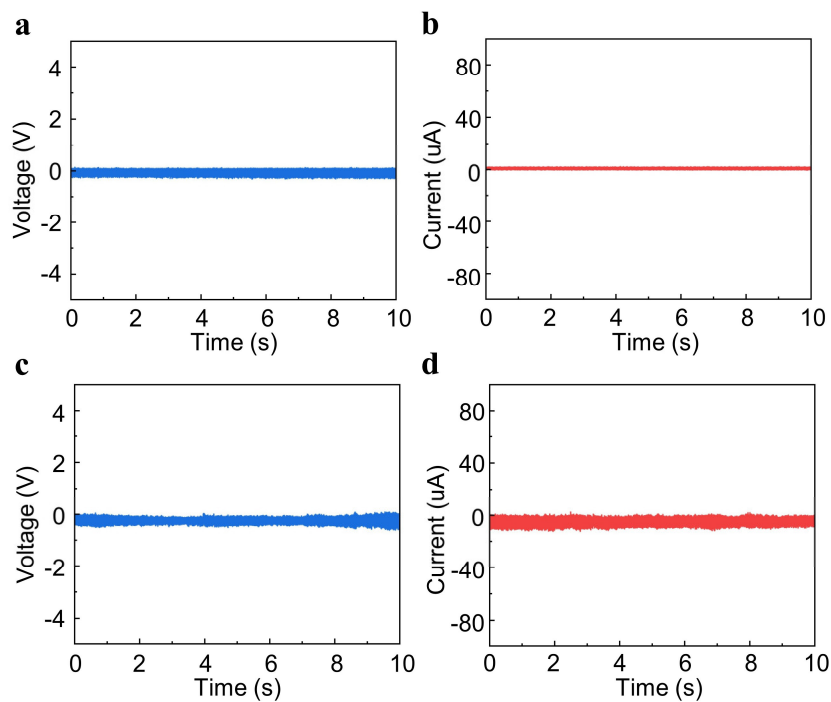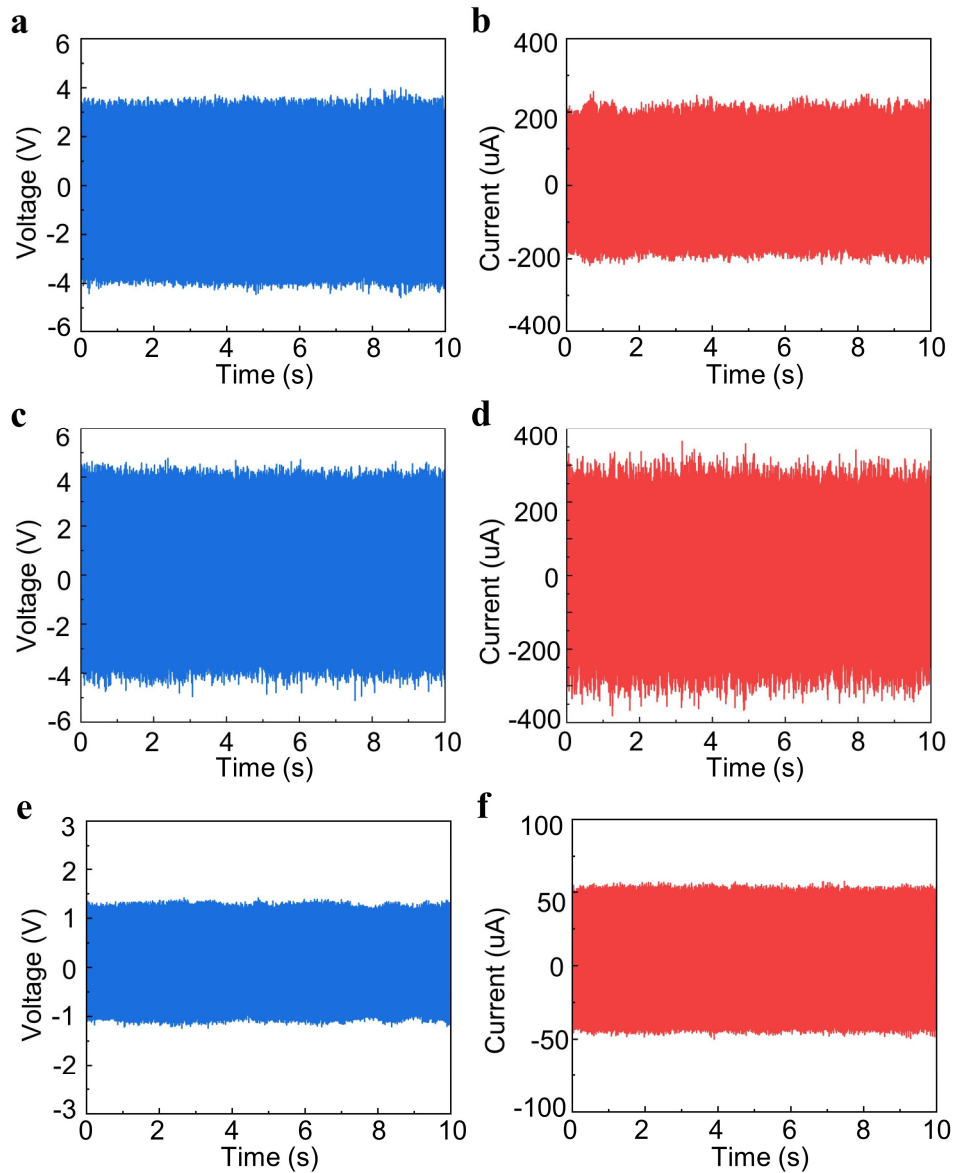
Fig. S16 Electrical characterization of pure PDMS and bulk PZT. (a and b) Open-circuit voltage signals (a) and short-circuit current signals (b) of pure PDMS. (c and d) Open-circuit voltage signals (c) and short-circuit current signals (d) of bulk PZT. The experimental setup is 18.5 mm, 40 kHz and 0.6 W cm^{-2}.
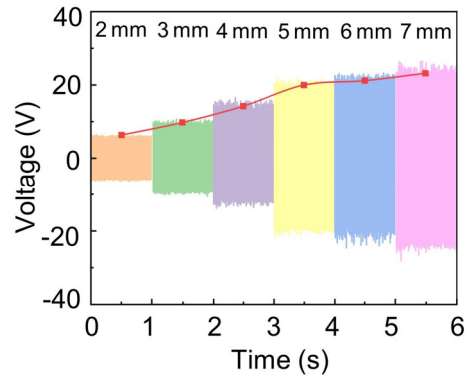
Fig. S17 Open-circuit output voltage signals of the W-PUEH (30×30 mm^2) under water with different thickness from 2 mm to 7 mm. The setup of the ultrasonic transmitter is 40 kHz and 0.6 W cm^{-2}. The distance is 18.5 mm.

Fig. S18 Electrical characterization *ex vivo*. (a and b) Open-circuit voltage signals (a) and short-circuit current signals (b) generated by the W-PUEH inserted under 5 mm porcine muscles. The experimental setup is 40 kHz and 0.6 W cm^{-2}. (c and d) Open-circuit voltage signals (c) and short-circuit current signals (d) generated by the W-PUEH inserted under 18.5 mm porcine muscles. The experimental setup is 40 kHz and 0.6 W cm^{-2}. (e and f) Output voltage signals (e) and current signals (f) generated by the W-PUEH inserted under 10 mm porcine muscles at 25 kΩ. The experimental setup is 40 kHz and 0.6 W cm^{-2}.
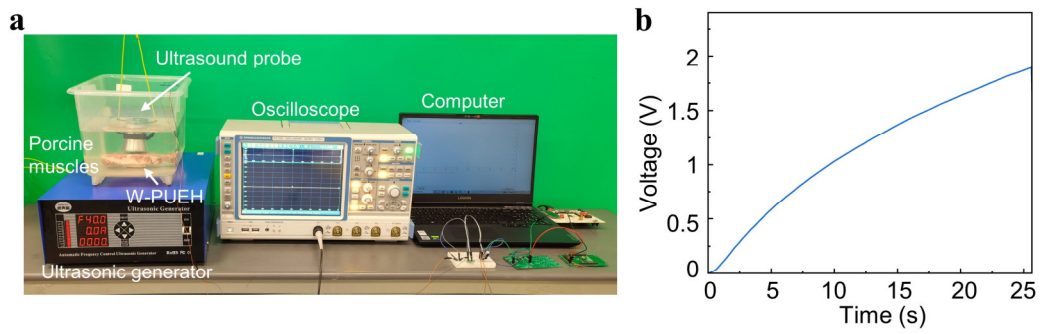
Fig. S19 Power generation ability of the W-PUEH through porcine tissue. (a) The setup of wireless signal transmission powered by the W-PUEH device under 10 mm porcine muscles. (b) The charging curve of 330 μF capacitor through 10 mm porcine muscles. The setup of the ultrasonic transmitter is 40 kHz and 0.6 W cm^{-2}.
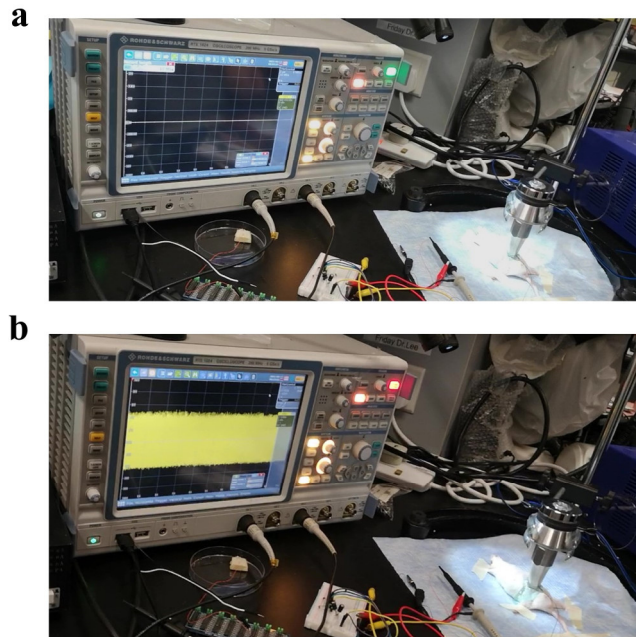
Fig. S20 The *in vivo* experimental setup. (a) Optical image showing the *in vivo* experimental setup without power input of the ultrasonic transmitter. No output signals are detected on the oscilloscope. (b) Optical image showing the *in vivo* experimental setup during wireless ultrasonic energy transfer. Obvious output signals (open-circuit voltage) are detected on the oscilloscope.
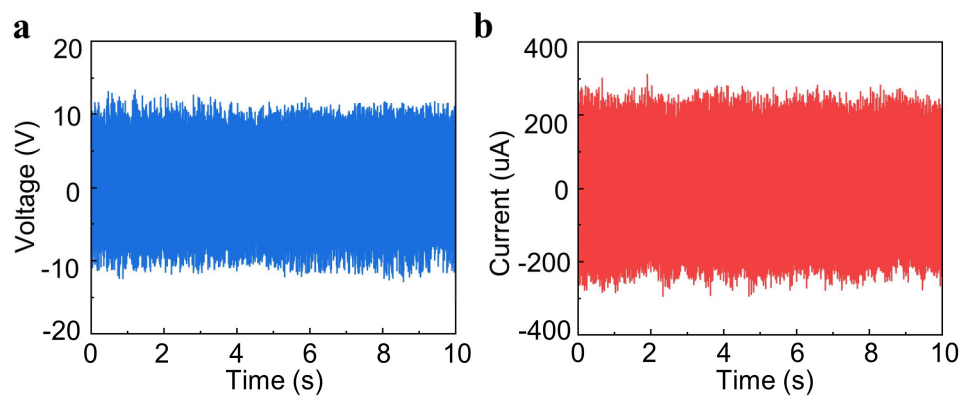
Fig. S21 Output voltage and current generated by the W-PUEH (15×15 mm^2) under US gel with a thickness of 3 mm. The transmitter setup is 40 kHz and 0.6 W cm^{-2}. The distance is 1 mm, same with the thickness of incised abdominal skin in the *in vivo* experiments.
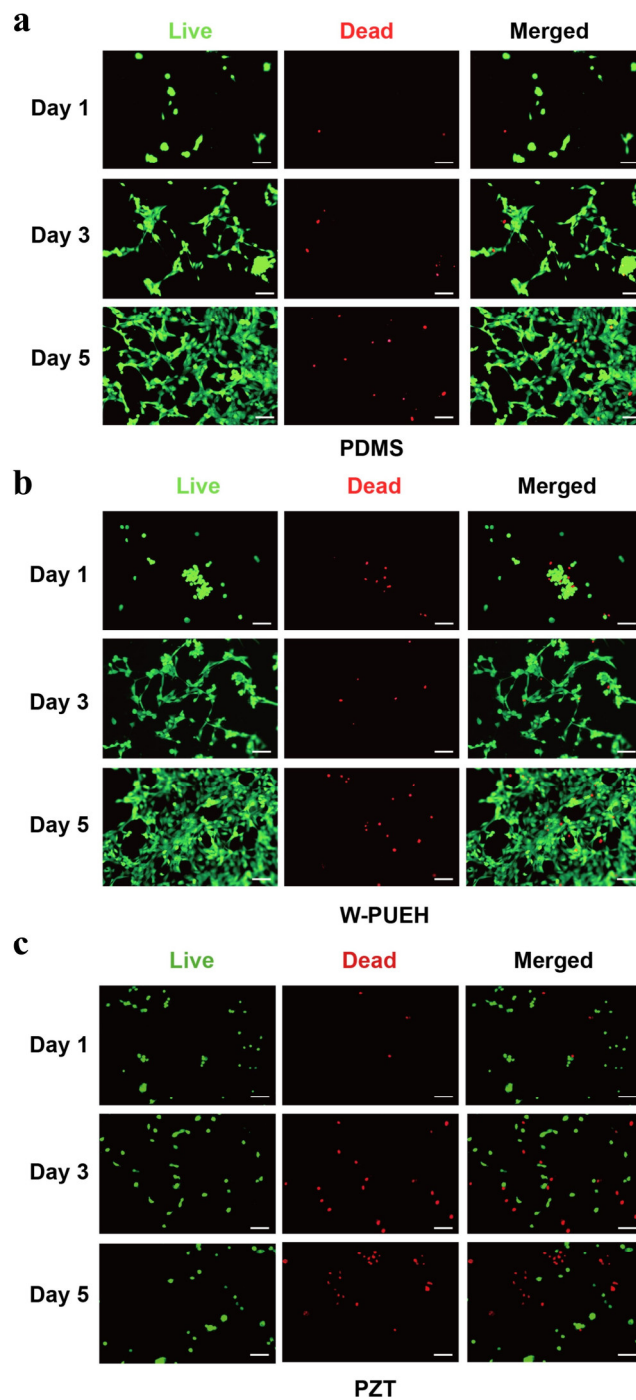
Fig. S22 Cell viability assay. (a) Fluorescent images of the myofibroblasts on the PDMS substrate on days 1, 3 and 5. Scale bar, 100 μm. (b) Fluorescent images of the myofibroblasts on the W-PUEH substrate on days 1, 3 and 5. Scale bar, 100 μm. (c) Fluorescent images of the myofibroblasts on the PZT substrate on days 1, 3 and 5. Scale bar, 100 μm.

Supplementary Tables

Table S1 Comparison of this work with ultrasonic energy harvesters previously reported.

Title	Output Voltage (V)	Output Current (μA)	Input Power Intensity (W cm⁻²)	Average Output Power Density (μW cm⁻²)	Conversion Efficiency (%)	Volumetric Energy Density (mW cm⁻³)	Flexible or Not
PZT film[59]	1.24	N/A	N/A	81.7*	0.013*	1.634*	N
PZT MEMs[38]	0.0021	0.04	0.001	2.05*	0.205*	2.05*	N
PZT crystal[32]	0.95	N/A	N/A	64*	0.00103*	0.163*	N
PZT array[40]	1.05	2.1	0.065	4.1	0.0063	0.114*	Y
VI-TEG[35]	9.71	427	3	67.3*	0.0022*	2.54*	N
μTUD[34]	0.0084	N/A	0.132	0.277*	0.00021	0.0033*	N
M-gel generator[26]	8	21	0.1	4.44*	0.0044*	0.044*	Y
This Work	**21**	**2000**	**0.6**	**304**	**0.051**	**0.608**	**Y**

* calculated from the corresponding data in the article. The average output power density is the instantaneous output power density divided by two.

N/A, not given in the article.

Definition of the six performance metrics in Fig. 3i, **Voltage**: Open-circuit voltage; **Power**: Average output power per unit area at matching impedance; **Efficiency**: Energy conversion efficiency, the ratio of output power density and input power intensity; **Distance**: Working distance between ultrasound probe and sample surface at maximum power output; **Flexible**: Easily bent or not; **Volumetric energy density**: Average output power per unit volume at matching impedance. The average output power P_{ave} is derived by

$$P_{ave} = \frac{\int_0^t \frac{V^2}{R}}{t} \tag{1}$$

where V is instantaneous output voltage, R is the external resistance, t is the working time.

Captions for Supplementary Movies

Movie S1

Finite element (FE) simulation of the acoustic field. The video shows the FE simulation of ultrasonic pressure propagation under water and ultrasonic-induced piezoelectric potential distribution in the W-PUEH.

Movie S2

12 LEDs lighted by the W-PUEH. The video shows 12 LEDs are lighted up by the W-PUEH. The video is at 1× playback speed.

Movie S3

Wireless signal transmission powered by the W-PUEH device *ex vivo*. The video shows the wireless signal transmission of the temperature signals obtained by a temperature sensor attached to the palm surface. The temperature variation of the palm surface is displayed on the computer screen. The video is at 50× playback speed.

Movie S4

Charging process during the wireless ultrasonic energy transfer *in vivo*. The video shows the charging process of a 100 µF capacitor during the wireless ultrasonic energy transfer *in vivo*. The generated power is able to charge the capacitor from 0 V to 1.55 V in 8 s. The video is at 1× playback speed.